Three-dimensional metrology and fractal analysis of dendritic nanostructures

Zineb Saghi,* Xiaojing Xu, and Günter Möbus
Department of Engineering Materials, University of Sheffield, Sheffield S1 3JD, United Kingdom
(Received 15 July 2008; revised manuscript received 12 September 2008; published 20 November 2008)

Three-dimensional quantification and fractal dimension analysis are performed on a nanoscale dendrite, grown by precipitation as a crystal from a glass matrix. In order to process the entire three-dimensional (3D) volume and surface properties, a reconstruction from multiple projections has been achieved using electron tomography. Digital evaluation of the 3D volume and surface of the reconstructed dendritic nanoparticle allows quantifying its surface-volume ratio, convexity, solidity, and fractal dimension. The structure is found fractal across much of the nanoscale, with a fractal dimension estimated to 2.4.

DOI: 10.1103/PhysRevB.78.205428 PACS number(s): 81.07.Bc, 81.70.Tx, 81.10.Aj

I. INTRODUCTION

The science of fractal structures has always fascinated researchers across multiple science disciplines. Besides some obvious naturally fractal objects such as coastal border lengths and snow flakes, fractality in practical materials of engineering importance has recently gained interest, as demonstrated in Refs. 1 and 2 and reviewed in Refs. 3 and 4. Fractal objects are more common in the macroworld. A basic requirement of an object to be fractal is its self-similarity across a certain length scale.[5] However, in the microscale and nanoscale, frequently encountered fractal objects are dendritic precipitates in their early stage of growth. These hyperbranched structures can be fabricated by supersaturation of a matrix, which cools faster than the precipitate itself, therefore favoring growth along any existing protrusions rather than spherical growth. The performances of these structures depend strongly on their morphology and dendritic growth directions. On the microscale, where the branches are already well developed, Granasy *et al.*[6] reported on the influence of impurities and crystallization temperature on the growth process, while Haxhimali *et al.*[7] demonstrated computationally the complexity and diversity of possible dendritic growth directions.

Fractal analysis is often carried out to quantitatively characterize the complex morphology of dendritic structures from transmission electron microscope (TEM) images.[8–10] Advances in instrumentation allow better understanding of the dendritic growth process with *in situ* TEM observation and fractal dimension evolution of the structures, as reported by Zhou *et al.*[11] However, TEM images only provide two-dimensional (2D) projections of dendritic structures, where individual branches cannot be all reliably identified. Quantitative parameters extracted from 2D images are not accurate as they depend strongly on the initial orientation of the structure, and the relationship between the fractal dimension of a three-dimensional (3D) object and the fractal dimension of its 2D projections can only be computationally estimated for simple morphologies.[12]

For a true 3D quantitative characterization, we propose here to use electron tomography (ET).[13] ET is a nondestructive technique which consists of reconstructing 3D volumes from a series of 2D TEM images taken at different tilt angles. ET has been recently transferred from biology[14] to materials science for the 3D reconstruction of, e.g., crystalline particles of a few hundred nanometers in diameter, with 1–5 nm resolution.[15–18] ET is usually employed for the 3D qualitative characterization of nanostructures. Recently, the capabilities of ET to provide valuable quantitative information have been demonstrated on block copolymers,[19] mesoporous silica,[20] and soot particles.[21]

In this paper, we employ ET for the 3D reconstruction and quantitative analysis of an isolated hyperbranched dendrite. The 3D dendritic growth directions are evaluated visually by surface rendering and slicing through the reconstructed volume. Several quantitative parameters of high relevance for industrial applications of nanocomposites describing the surface and volume properties of the dendrite are extracted from the tomogram, and fractal analysis is employed to evaluate the self-similarity and surface irregularities of the 3D structure.

II. MATERIALS AND METHODS

Precipitation of dendrites was induced by doping of an alkali borosilicate base glass. The glass was prepared with 8.6 Na_2O, 4.3 Li_2O, 25.7 B_2O_3, and 51.4 SiO_2 (mol %) base glass matrix with 4.0 CeO_2, 2.0 Cr_2O_3, and 4.0 ZrO_2 (mol %) dopants added. The glass was placed in a platinum crucible and melted at 1400 °C for 5 h and annealed at 570 °C for 1 h, followed by a cooling to room temperature at a rate of 1 °C/min. The bulk glass was ground in acetone and the resulting suspended glass fragments were dropped onto a carbon grid for their microstructural analysis. The tomographic experiment was carried out in a JEM 2010F field-emission gun TEM (Jeol, Japan) operating at 200 kV with a 2 mm ultraresolution pole piece gap. We used annular dark field scanning TEM (ADF-STEM) imaging mode for the image acquisition as it has two advantages: (1) the incoherent nature of this mode fulfills the projection requirement, i.e., linearity between the projected signal and the atomic number density of the specimen, which is a prerequisite for reliable tomography reconstruction and (2) the projected signal is proportional to nearly the square of the atomic number. As there is a high atomic number difference between Ce and the matrix glass, ADF-STEM images exhibit a high contrast, as seen in the ADF-STEM image of a Ce-loaded borosilicate glass in Fig. 1(a). Previous work[22] showed that tomographic

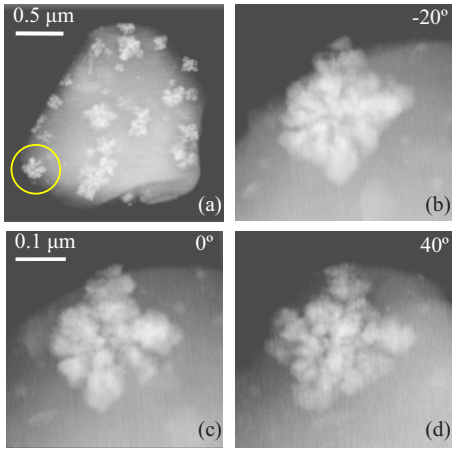

FIG. 1. (Color online) (a) Glass fragment with CeO_2 precipitates. The dendrite encircled was selected for the tomographic analysis at high magnification. (b), (c), and (d) are projections from the tilt series of the dendrite at −20°, 0°, and +40°, respectively. All images were recorded using ADF-STEM (Z contrast).

reconstruction of the whole fragment gives valuable information about the size, volume fraction, and the distribution homogeneity of the CeO_2 precipitates. In this work, we were interested in the detailed quantitative structural characterization of the isolated 200-nm-diameter dendrite encircled in Fig. 1(a). A tomography holder (Gatan model 912) was used for the tilt series acquisition from −70° to +70° with 5° increment. The recorded images were then exported to IMOD (Ref. 23) for cross-correlation alignment, and the tomographic reconstruction was achieved by the filtered back-projection algorithm using the same software. Qualitative visual evaluation by surface rendering and slicing through the tomogram was achieved using AMIRA software (Mercury Computer Systems, USA), while the quantitative postprocessing was done in Interactive Data Language (ITT Systems, USA). The reconstructed volume was binarized by smoothing and global thresholding so as to separate the pixels that belong to the dendrite (pixel value 1) from those that belong to the glass matrix (pixel value 0). The convex hull V_h of the binarized volume V_d, defined as the smallest convex set containing V_d, was obtained by the shape-from-silhouette (SFS) algorithm. We reprojected V_d from −90° to +90° with 1° increment after applying a closing morphological operation in order to remove the remaining noise and regularize the boundary. The projections were then binarized to obtain the silhouettes and back projected. The intersection of all back-projected silhouettes defines the convex hull V_h. We denote S_s as the binarized central slice through V_d and S_h its convex hull. First, the area A_{ss} and the volume V_{vd} were obtained by multiplying the total number of nonzero pixels by the pixel and voxel dimensions in A_s and V_d, respectively. The perimeter P_{ss} and surface S_{vd} of S_s and V_d were extracted from the edge-enhanced versions of S_s and V_d. Similar processing was then applied to S_h and V_h to estimate the convex area A_{sh} and perimeter P_{sh} and the convex volume V_{vh} and surface S_{vh}.

In addition to surface and volume measurements, four appropriate parameters were selected to assess the structure and texture of the selected 2D slice S_s and the 3D overall dendritic structure V_d:

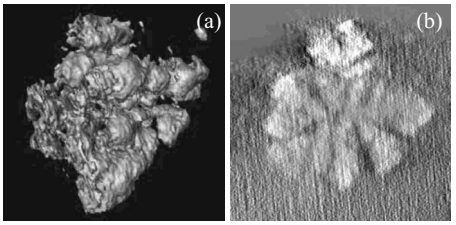

FIG. 2. (a) Isosurface of the reconstructed dendrite and (b) a slice through the tomogram showing the orientation of individual branches.

(i) *Perimeter/area ratio* (P_{ss}/A_{ss}) and surface/volume ratio (A_{ss}/V_{vd}). This parameter, although not dimensionless, is easy to measure and sensitive to all kinds of deviations of a surface from a sphere, which would have minimum ratio. As it indicates how much surface per unit volume of material is generated, it is very widely used in surface active research and industrial fields of applications, e.g., catalysis, and often expressed as surface/mass.

(ii) *Solidity.* Defined as the area/(convex area) ratio in 2D (A_{ss}/A_{sh}) or volume/(convex volume) ratio in 3D (V_{vd}/V_{vh}), this parameter quantifies the extent to which the feature area or volume covers the convex hull area or volume. It is equal to 1 for a convex particle and less for particles with concavities and as such measures the porosity or hollowness of materials. It differs from (i) as it is constant for different convex shapes. Unlike (iii) below, it is not sensitive to the aspect ratio of concavities.

(iii) *Convexity.* Defined as the (convex perimeter)/perimeter ratio in 2D (P_{sh}/P_{ss}) or the (convex surface)/surface ratio in 3D (A_{sh}/A_{ss}), the convexity is similar to the solidity parameter but is more sensitive to deep and narrow intrusions as these significantly increase the perimeter (2D) or surface (3D).

(iv) *Fractal dimension.* This parameter is used for quantitative analysis of the self-similarity of particles. The fractal dimension Df is estimated here using the box counting method, where the number $N(L)$ of boxes of side length L required to cover the 2D slice or the 3D tomogram is calculated as the boxes are made finer. If the particle is fractal, its fractal dimension Df is nonintegral and defined as the slope of the linear part of the log-log plot,

$$Df = \lim_{L \to 0} \frac{\log_{10} N(L)}{\log_{10}(1/L)}. \quad (1)$$

III. RESULTS AND DISCUSSION

Figures 1(b)–1(d) are the ADF-STEM images of the selected dendrite at −20°, 0°, and +40° tilt angles, respectively. These images show the branching morphology and the preferred growth directions of the dendrite. The isosurface representation of the reconstructed tomogram is shown in Fig. 2(a) while the 2D central slice through the volume [Fig. 2(b)] shows the high fractal fragmentation of the dendrite. The

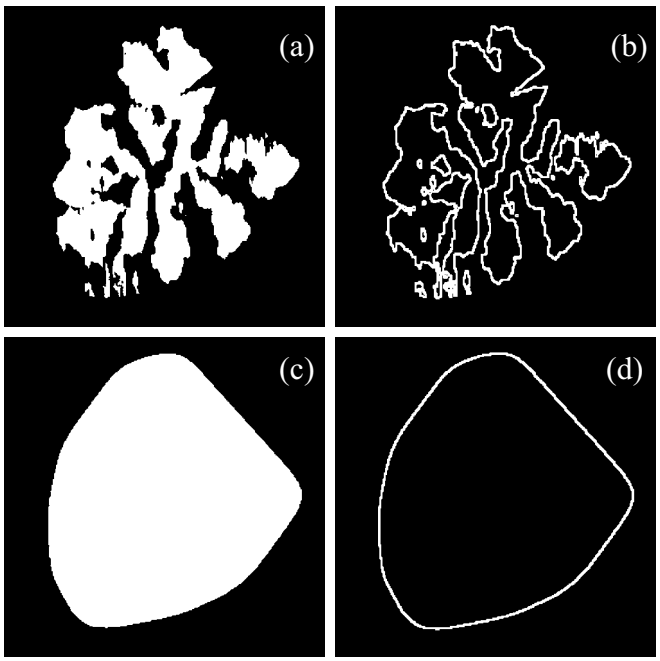

FIG. 3. (a) Binarized and (b) edge-enhanced versions of the slice in Fig. 2(b). The convex hull of (a) was (c) extracted and (d) edge enhanced.

volume can be rotated and sliced through different directions and planes to allow a full qualitative assessment of the growth directions and dendritic branching. This visual information is unavailable on 2D TEM projections where individual branches growing in different 3D directions are overlapped.

For the quantitative analysis of the dendrite structure, smoothing with a median filter and binarization were applied to the tomogram to extract the 3D dendrite from the glass matrix. The segmented version of the 2D slice in Fig. 2(b) is represented in Fig. 3(a), where the branches are now better visible. A Sobel high-pass filter was applied to the segmented tomogram, as seen in Fig. 3(b). The convex hull and its edge-enhanced version were also determined by shape-from-silhouette technique and Sobel filtering, respectively. Figure 3(c) is the convex hull of Fig. 3(a) while the edge-enhanced version of Fig. 3(c) is the contour envelop of the structure [Fig. 3(d)]. The quantitative data estimated for the segmented 2D central slice [Fig. 3(a)] and the 3D volume are summarized in Table I. The 2D parameters extracted from any single slice through the volume can give insight into the dendritic growth process in the chosen 2D plane. This quantitative information is specific to one single slice and is not based on projections anymore. The perimeter/area ratio of the 2D slice is found to be 0.25 nm^{-1} while the surface/volume ratio of the 3D tomogram is 0.26 nm^{-1}. The corresponding values for a circle and a sphere of 150 nm radius would be 0.013 and 0.02 nm^{-1}, respectively. The solidity parameter was measured as 0.53 for the 2D slice and 0.48 for the total volume. This important result quantifies the glass/crystal ratio within the envelope of the dendrite to nearly 50% glass and 50% crystal. The dendrite has consequently rather thick branches and sub-branches within each individual branch to fill space, as a more finely architectured (snowflakelike) dendrite would result in a solidity value much smaller than 50%. This parameter however does not distinguish between few thick and many dense small branches (or deepness of intrusions). A more suitable parameter for quantifying the coarseness of the branches is the convexity. This parameter was found equal to 0.27 for the 2D slice and 0.36 for the 3D dendrite. These low values clearly demonstrate that the branches enlarge contours by a factor of 4 (2D) or 3 (3D) compared to a spherical precipitate of the same size. This corresponds to a diversity of individual branches, with deep and narrow channels separating them from each other. Low convexity values finally suggest that the dendrite is possibly fractal, as this is a necessary condition for this type of structures. To answer this final characteristic parameter, Figs. 4(a) and 4(b) present the box counting plots of the 2D slice and the 3D dendrite, respectively. The linear profiles of both plots, reliably including the range of 3–50 nm, suggest that the limit in Eq. (1) is finite, which is a proof of the fractal nature of the structures over this length scale. The fractal dimension Df was found to be 1.6 for the 2D slice and 2.4 in 3D. In combination with direct observation of the complex dendritic growth on Fig. 2(b) with the nested structure of main branches and sub-branches, we can confirm meaningful interpretation of the mathematical estimates for fractal dimension, which in itself would not be sufficient to prove the fractal nature. To relate these results to those of nonfractal objects, the fractal dimension of the convex support was estimated to be 1.94 and 2.96 for the 2D slice [Fig. 3(c)] and 3D volume, respectively. These values are very close to the ones of a regular square ($Df=2$) and cube ($Df=3$), as expected visually from the shapes of the 2D

TABLE I. Summary of the quantitative analysis of the 2D slice and the 3D dendrite.

Property	2D	Property	3D
Area (nm^2)	37050	Volume (nm^3)	7576500
Perimeter (nm)	9188	Surface (nm^2)	1992000
Convex perimeter (nm)	2525	Convex surface (nm^2)	712300
Convex area (nm^2)	69912	Convex volume (nm^3)	15820000
Perimeter/area (nm^{-1})	0.25	Surface/volume (nm^{-1})	0.26
Solidity	0.53	Solidity	0.48
Convexity	0.27	Convexity	0.36
Fractal dimension	1.6	Fractal dimension	2.4

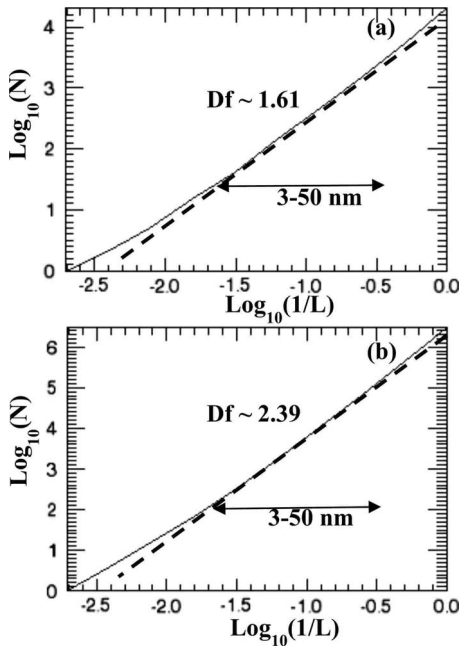

FIG. 4. (a) 2D and (b) 3D box counting plots of $\log_{10}(n)$ vs $\log_{10}(1/L)$. The logarithms are base 10. *Df* values correspond to the fractal dimensions obtained by estimating the slope of the linear part of the curves (dashed lines). The fractality holds for a length scale from 3 to 50 nm.

and 3D envelopes. The fractal analysis method presented here will allow to study the 3D morphology development during more extended annealing sequences as a function of time and therefore learn about the nature of dendritic particle growth at any convenient scale after completion of the nucleation process.

The resolution of the ADF-STEM reconstruction is estimated to 5 nm^3. Many factors certainly influence the accuracy of the parameters given in Table I. The limited angular range in the tilt series acquisition (from −70° to +70°) induces an elongation of the structure by a factor of 1.3 in the missing directions, leading to an overestimation of the volume and surface values. As the SFS technique is also affected by the missing wedge, this overestimation concerns also the volume and surface values of the convex envelop. The threshold value chosen for the volume segmentation changes significantly the results in Table I. Because of the noisy background representing the glass matrix [Fig. 2(c)], a low-pass filtering was applied to the volume and a global threshold value was chosen visually as a compromise between the background suppression (high threshold value) and the inclusion of all voxels belonging to the material (low threshold value). To estimate the thresholding error made on the parameters in Table I, different threshold values were chosen within the interval where the branches interconnectivity was respected. The error on the surface and perimeter was found to be 2.5% and 1.5%, respectively. By adding the fractional uncertainties in quadrature, we found an error of 2.9% in the perimeter/area parameter, 3.5% in the solidity, and 2.1% in the convexity. The fractal dimension is not as much subject to the threshold fluctuations, as the box counting method is based on averaging. This parameter is rather affected by the evaluation of the slope in Fig. 4, which was found to have an accuracy of ±0.1. All the presented error estimations were performed on the central cross section in Fig. 2(b) but can be extended to all slices and ultimately to the 3D parameters, as the back-projection algorithm reconstructs the tomogram slice by slice. More robust noise filtering and thresholding techniques[13] are expected to reduce the segmentation uncertainties in the results.

IV. CONCLUSION

Electron tomography was used for the 3D reconstruction of a single dendrite embedded in a glass matrix. Appropriate parameters were selected for the 3D analysis of the shape and texture of such particles. Various branches were found to be individually developed, with concavities at their surfaces. The dendrite was also found to be of a fractal nature, with self-similarities at different scales. In spite of the uncertainties due to the segmentation technique, the 3D analysis of dendritic structures by ET is more reliable than 2D quantification on TEM projections. The 3D morphology of dendritic crystals was shown to be more complex than expected.[7] Both 3D qualitative and quantitative information about these complex structures will certainly complement computer simulation for a better understanding and a more accurate prediction of the dendritic growth in 3D.

ACKNOWLEDGMENT

This work was supported by a grant from the EPSRC-GB Basic Technology Programme (Grant No. GR/S85689/01).

*z.saghi@sheffield.ac.uk

[1] K. Amano, D. Narimatsu, S. Sotome, S. Tashiro, A. Uchida, and S. Yoshimori, Phys. Rev. E **76**, 046213 (2007).
[2] R. P. Taylor, R. Newbury, A. S. Sachrajda, Y. Feng, P. T. Coleridge, C. Dettmann, N. Zhu, H. Guo, A. Delage, P. J. Kelly, and Z. Wasilewski, Phys. Rev. Lett. **78**, 1952 (1997).
[3] J. L. Vehel, E. Lutton, and C. Tricot, *Fractals in Engineering: From Theory to Industrial Applications* (Springer-Verlag, Berlin, 2000).
[4] H. Diab and N. Abboud, Simulation **57**, 89 (1991).
[5] B. Mandelbrot, *The Fractal Geometry of Nature* (Freeman, San Francisco, 1982).
[6] L. Granasy, T. Pusztai, T. Borzsonyi, J. A. Warren, and J. F. Douglas, Nature Mater. **3**, 645 (2004).
[7] T. Haxhimali, A. Karma, F. Gonzales, and M. Rappaz, Nature Mater. **5**, 660 (2006).
[8] D. A. Weitz and M. Oliveria, Phys. Rev. Lett. **52**, 1433 (1984).
[9] G. Radnoczi, T. Vicsek, L. M. Sander, and D. Grier, Phys. Rev.

A **35**, 4012 (1987).
[10] R. He, X. Qian, J. Yin, and Z. Zhu, Chem. Phys. Lett. **369**, 454 (2003).
[11] G.-W. Zhou, L. Wang, R. C. Birtcher, P. M. Baldo, J. E. Pearson, J. C. Yang, and J. A. Eastman, Phys. Rev. Lett. **96**, 226108 (2006).
[12] C. Lee and T. A. Kramer, Adv. Colloid Interface Sci. **112**, 49 (2004).
[13] J. Frank, *Electron Tomography: Methods for Three-Dimensional Visualization of Structures in the Cell*, 2nd ed. (Plenum, New York, 2007).
[14] A. J. Koster, R. Grimm, D. Typke, R. Hegerl, A. Stoschek, J. Walz, and W. Baumeister, J. Struct. Biol. **120**, 276 (1997).
[15] G. Möbus, R. D. Doole, and B. J. Inkson, Ultramicroscopy **96**, 433 (2003).
[16] P. A. Midgley and M. Weyland, Ultramicroscopy **96**, 413 (2003).
[17] G. Möbus and B. J. Inkson, Appl. Phys. Lett. **79**, 1369 (2001).
[18] Z. Saghi, X. Xu, Y. Peng, B. J. Inkson, and G. Möbus, Appl. Phys. Lett. **91**, 251906 (2007).
[19] H. Jinnai, T. Kajihara, H. Watashiba, Y. Nishikawa, and R. J. Spontak, Phys. Rev. E **64**, 010803(R) (2001).
[20] E. P. W. Ward, T. J. V. Yates, J.-J. Fernandez, D. E. W. Vaughan, and P. A. Midgley, J. Phys. Chem. C **111**, 11501 (2007).
[21] K. Adachi, S. H. Chung, H. Friedrich, and P. R. Buseck, J. Geophys. Res. **112**, D14202 (2007).
[22] G. Möbus, G. Yang, Z. Saghi, X. Xu, R. J. Hand, A. Pankov, and M. I. Ojovan, *Scientific Basis for Nuclear Waste Management XXXI*, MRS Symposia Proceedings No. 1107 (Materials Research Society, Pittsburgh, 2007).
[23] J. R. Kremer, D. N. Mastronarde, and J. R. McIntosh, J. Struct. Biol. **116**, 71 (1996).